Single-Step Delamination of a MWW Borosilicate Layered Zeolite Precursor under Mild Conditions without Surfactant and Sonication
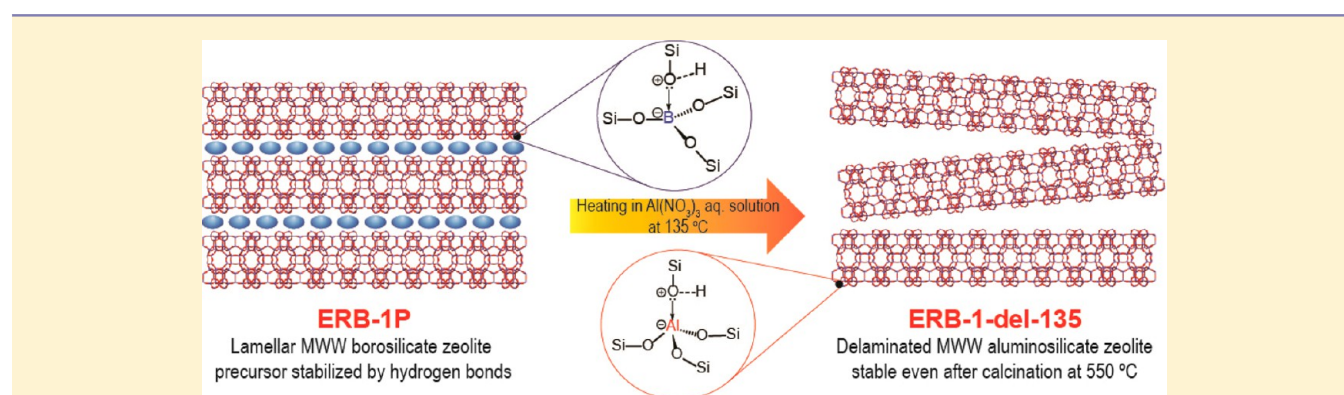
Xiaoying Ouyang,[†] Son-Jong Hwang,[‡] Ron C. Runnebaum,[†] Dan Xie,[§] Ying-Jen Wanglee,[†] Thomas Rea,[§] Stacey I. Zones,*[,†,§] and Alexander Katz*[,†]

[†]Department of Chemical and Biomolecular Engineering, University of California at Berkeley, Berkeley, California 94720, United States

[‡]Department of Chemical Engineering, California Institute of Technology, Pasadena, California 91125, United States

[§]Chevron Energy Technology Company, Richmond, California 94802, United States

S *Supporting Information*

ERB-1P
Lamellar MWW borosilicate zeolite precursor stabilized by hydrogen bonds

Heating in Al(NO₃)₃ aq. solution at 135 °C

ERB-1-del-135
Delaminated MWW aluminosilicate zeolite stable even after calcination at 550 °C

ABSTRACT: Layered borosilicate zeolite precursor ERB-1P (Si/B = 11) is delaminated via isomorphous substitution of Al for B using a simple aqueous $Al(NO_3)_3$ treatment. Characterization by PXRD shows loss of long-range order, and TEM demonstrates transformation of rectilinear layers in the precursor to single and curved layers in the delaminated material. N_2 physisorption and base titration confirm the expected decrease of micropore volume and increase in external surface area for delaminated materials relative to their calcined 3D zeolite counterpart, whereas FTIR and multinuclear NMR spectroscopies demonstrate synthesis of Brønsted acid sites upon delamination. Comparative synthetic studies demonstrate that this new delamination method requires (i) a borosilicate layered zeolite precursor, in which boron atoms can be isomorphously substituted by aluminum, (ii) neutral amine pore fillers instead of rigid and large quaternary amine SDAs, and (iii) careful temperature control, with the preferred temperature window being around 135 °C for ERB-1P delamination. Acylation of 2-methoxynaphthalene was used as a model reaction to investigate the catalytic benefits of delamination. A partially dealuminated delaminated material displays a 2.3-fold enhancement in its initial rate of catalysis relative to the 3D calcined material, which is nearly equal to its 2.5-fold measured increase in external surface area. This simple, surfactant- and sonication-free, mild delamination method is expected to find broad implementation for the synthesis of delaminated zeolite catalysts.

■ INTRODUCTION

Though zeolites exhibit catalytic utility and shape selectivity due in large part to their well-defined active sites, which consist of heteroatoms substituted within framework positions, to date, the scope of this catalysis has largely been limited to small molecules that can fit inside of micropores, where the vast majority of active sites are located. Expanding the scope of zeolite catalysts to include larger molecules has motivated the elegant synthesis and discovery of several classes of zeolite-based materials such as extra-large-pore zeolites,[1,2] delaminated layered zeolite precursor materials,[3-8] single-unit-cell zeolite nanosheets,[9] hierarchically nanoporous zeolite-like materials,[10,11] and self-pillared zeolite nanosheets.[12] However, all of these, while beautiful in their own right, require an intricate self-assembly between organic surfactants and inorganic zeolite

framework in order to function synthetically. These surfactants are costly and render the process of accessible zeolite synthesis less atom efficient, since they are typically irreversibly consumed (e.g., combusted during calcination) prior to use. Recently, in order to overcome this, there have been great interest and an emergence of approaches for synthesis of accessible zeolitic structures that do not require organic surfactants. Relevant examples include synthesis of MCM-56 analogues, which use mild acid treatment of as-made MWW layered zeolite precursors for removing structure-directing agent (SDA) and consist of disordered zeolite-layer sheets. These materials catalyze reactions with sterically bulky reactants
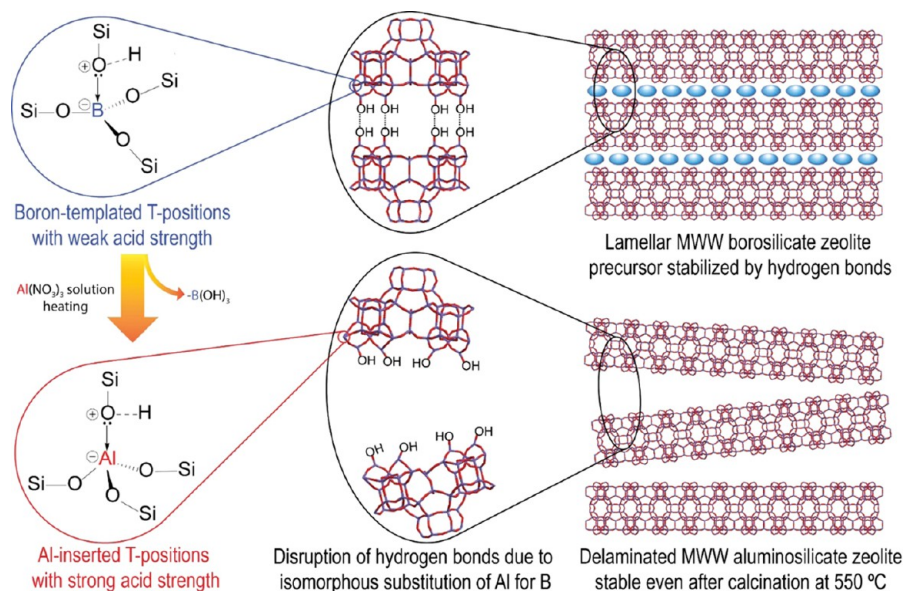
Figure 1. Schematic diagram of the surfactant-free exfoliation of a MWW-type borosilicate zeolite precursor into a delaminated aluminosilicate zeolite in a single step.

that are unable to access active sites within internal micropores, such as Ti-catalyzed epoxidation of cyclooctene using *tert*-butylhydroperoxide as oxidant, Al-catalyzed cracking of 1,3,5-triisopropylbenzene, and Sn-catalyzed Baeyer−Villiger oxidation of 2-adamantanone.[13−15] Another approach for synthesis of accessible zeolites without organic surfactants has been the transformation of three-dimensional (3D) UTL germanosilicate into a two-dimensional (2D) lamellar zeolite by Čejka et al., who demonstrated that zeolite layers become separated during hydrolysis of the double-four ring (D4R) bridging units,[16−18] and these disassembled layers can be reassembled by intercalating diethoxydimethylsilane, to form zeolites with unique channel systems, such as IPC-2 and IPC-4.[19] This latter approach, while elegant, requires precursors that consist of unique Ge-containing D4R units in the space between layers, such that D4R removal via hydrolysis results in 2D zeolite layers.

Here, in this contribution, we demonstrate the simplest method yet reported for imparting greater accessibility into zeolitic materials via delamination, which does not require either organic surfactants, corrosive pH (which can lead to amorphization of the zeolite framework), or energy-intensive sonication in order to achieve delamination. Our method is accomplished in a single-step via an extraordinarily simple treatment with a warm metal-salt solution at mild pH of around 3. We demonstrate our approach via exfoliation of a borosilicate layered zeolite precursor ERB-1P (uncalcined material that consists of a high amount of piperidine (PI) remaining in the zeolite host lattice, with Si/B = 11), which has an MWW topology, as shown in Figure 1. We synthesize new delaminated zeolitic materials that consist of a topology similar to those previously described, such as ITQ-2[3] and UCB-1,[5] which also originate from an MWW-type layered zeolite precursor but require either organic surfactants and/or corrosive pH and sonication for delamination to occur. Delamination of ERB-1P is accomplished via treatment of the layered borosilicate zeolite precursor with a heated Al(NO$_3$)$_3$ aqueous solution under autogenous pressure, during which time interlayer hydrogen bonding in the precursor becomes permanently disrupted (i.e.,

this disruption persists even after calcination of the material at 550 °C) and is accompanied by isomorphous substitution of Al for B in framework T-positions. We believe that the permanence of our delamination approach is facilitated by lattice distortions along both the *c*-axis and the *a*−*b* plane, which are induced by substitution of Al for B. The delaminated zeolitic materials resulting from our approach are active catalysts for Friedel−Crafts acylation (FCA) of 2-methoxynaphthalene (2MN) with acetic anhydride (Ac$_2$O), which occurs exclusively on external acid sites. Our results demonstrate that the observed rate of catalysis is not only sensitive to external acid-site density but also to acid-site proximity and presence of octahedral extra-framework Al species.

Though borosilicate zeolites have generally been considered less useful in acid catalysis because of their intrinsically weak acidity,[20−22] from a materials synthesis perspective, these are unique materials in which B can be substituted with other heteroatoms in the framework, such as Al,[23,24] Ga,[23] and Ti,[25−27] among others. The resulting heteroatom-substituted metallosilicate zeolites consist of metals within specific framework positions, which may otherwise be difficult to achieve via direct synthesis,[23] since the B atoms essentially template metal heteroatom binding to certain T-positions within the zeolitic framework. Alternatively, if no metal heteroatom is rebound to the framework during deboronation, silanol nests can be created.[28,29] Such silanol nests can in principle serve as tetrahedral recognition binding sites that can be subsequently reoccupied by another metal ion (M), which has a size and oxygen coordination geometry (bond lengths and angles) similar to those of B in the framework and forms tetrahedral MO$_4$ sites.

Chen et al. previously investigated cation exchange in calcined 3D borosilicate zeolites, e.g., B-SSZ-33, and reported that treatment of these zeolites with Al(NO$_3$)$_3$ solution in a single step successfully exchanges B located within 12-membered rings (12-MR) of the framework with Al.[23] Data from Chen et al. also suggest that it may be impossible to exchange B sites that are located in 10-MR for Al, presumably

due to the bulkiness of the hydrated $Al(H_2O)_6^{3+}$ cations, since it was not possible to exchange Al for B sites in ZSM-11, which consists entirely of 10-MR.[23] The resulting materials after Al exchange for B exhibit the type of strong Brønsted acidity typically associated with Al-acid sites within a zeolitic framework.[30] Such sites are known to be difficult to synthesize with the same degree of uniformity and acid-site density when using amorphous silica–alumina materials.

■ EXPERIMENTAL SECTION

Materials. All reagents used throughout were of reagent-grade quality and were used as-received unless otherwise noted. Acridine (97%, Sigma-Aldrich) was recrystallized in ethanol twice before use for titration of external acid sites.

Synthesis of ERB-1 Precursor (ERB-1P). Synthesis of ERB-1P was performed on the basis of the reported literature procedure, with minor modifications.[31] Typically, 2.40 g of NaOH (EMD Chemicals, 97%) and 6.18 g of H_3BO_3 (≥99.5%, Fisher Chemical) were dissolved in 30 mL of nanopure H_2O, and 12.8 g of PI (≥99.5%, purified by redistillation, Sigma-Aldrich). To this mixture were added 9.0 g of SiO_2 (Aerosil 200, Evonik-Degussa) and 0.10 g of seed crystals (as-made ERB-1P, Si/B = 11). A white viscous gel was obtained after mixing with a spatula. The gel composition in molar ratios was SiO_2:0.33 B_2O_3:0.2 Na_2O:1.0 PI:11.0 H_2O. This gel was subsequently transferred to a 125 mL Parr reactor equipped with a Teflon liner. The reactor was heated at 175 °C for a period of 7–9 days without agitation. After cooling, the contents were poured into a filter, and the precipitated solids were washed several times with water and then air-dried.

Synthesis of ERB-1C. The air-dried ERB-1P was calcined in air at 550 °C for 5 h.

Synthesis of ERB-1C-Al. In a typical procedure, 1.0 g of ERB-1C was added to 100 g of 0.4 N $Al(NO_3)_3$ aqueous solution in a 250 mL, sealed, thick-walled glass reactor with vigorous stirring. The mixture was heated and maintained at 100 °C for 4 days. The solid product was collected on a filter, washed consecutively with pH 2 HCl solution and water, air-dried, and subsequently calcined at 550 °C for 5 h in air.

Synthesis of MCM-22P. MCM-22P was synthesized according to literature procedure.[4] The gel composition in molar ratios was SiO_2:0.011 Al_2O_3:0.079 Na_2O:0.49 hexamethyleneimine (HMI):44 H_2O. The reaction was conducted in a convection oven at 135 °C for 11 days, with tumbling of the reactor.

Synthesis of B-SSZ-25. B-SSZ-25 was synthesized according to literature procedure.[32] The gel composition in molar ratios was SiO_2:0.07 B_2O_3:0.32 NH_4F:0.32 N,N,N-trimethyl-8-ammoniumtricyclo[5,2,1,0] decane:5 H_2O. The reaction was conducted in a convection oven at 160 °C for 6 days, with tumbling of the reactor.

Synthesis of B-SSZ-70. 1,3-Diisobutylimidazolium (SDA) hydroxide solution for the synthesis of B-SSZ-70 was prepared as described in the literature.[8,33] Synthesis of B-SSZ-70 was performed according to a previously published method.[8] The gel composition in molar ratios was SiO_2:0.033 B_2O_3:0.050 Na_2O:0.20 SDA:30 H_2O. The reaction was conducted at 150 °C for 7 days, with tumbling of the reactor.

Delamination of Zeolite Precursors. In a typical procedure, 1.0 g of zeolite precursor was added to 100 g of 0.4 N $Al(NO_3)_3$ aqueous solution in a 250 mL, sealed, thick-walled glass reactor with vigorous stirring. The mixture was heated and maintained at various temperatures, including 100, 135, 150, and 175 °C. Materials resulting from this treatment are denoted as ERB-1-del-100, ERB-1-del-135, ERB-1-del-150, and ERB-1-del-175, respectively. The solid products were collected on a filter, washed thoroughly with water, air-dried, and subsequently calcined at 550 °C for 5 h in air.

Dealumination of ERB-1-del-135. In a typical procedure, 0.25 g of ERB-1-del-135 was added to 2 mL 1 N HNO_3 solution in a 15 mL, sealed, thick-walled glass reactor with vigorous stirring. The mixture was heated at 100 °C for 1 h before being collected on a filter, washed thoroughly with water, and air-dried. The resulting material is denoted as ERB-1-del-135D.

Characterization Methods. Powder X-ray diffraction (PXRD) patterns were collected on a Bruker GADDS D-8 diffractometer using a Cu Kα radiation. Data were collected in the 2θ range from 3° to 30° with a step size of 0.02° and a dwell time of 2 s. LeBail-type whole-pattern profile-fitting[34,35] was performed using the GSAS-EXPGUI software package.[36,37] The peak shape function used to fit the powder patterns is the modified Thompson–Cox–Hastings pseudo-Voigt function.[38] Peak asymmetry due to axial divergence was calculated by the model proposed by Finger et al.[39]

General. The Si and Al contents of all materials were determined using Inductive Couple Plasma Mass Spectroscopy (ICP-MS) analysis conducted at Galbraith Laboratories, USA. Transmission electron microscopy (TEM) images were recorded on a JEOL JEM-2010 (200 kV) at Chevron Energy Technology Company. Nitrogen physisorption isotherms were measured on a Micromeritics ASAP2020 instrument at 77 K. Prior to measurement, samples were evacuated at 350 °C for 4 h. The pore size distributions were calculated by the nonlocal density functional (NLDFT) method[40] based on the adsorption data. Multinuclear solid state NMR experiments were performed for ^{11}B, ^{27}Al, and ^{29}Si nuclei at ambient conditions using a Bruker Avance 500 MHz spectrometer with a wide-bore 11.7 T magnet and employing a 4-mm MAS probe (Bruker). The spectral frequencies were 160.5, 130.5, and 99.4 MHz for the ^{11}B, ^{27}Al, and ^{29}Si nuclei, respectively. Short single pulses (0.5 μs-18° for ^{11}B or 10° for 27Al) followed by strong ^1H decoupling (rf ∼100 kHz) were used for both ^{11}B and ^{27}Al MAS NMR measurements at the sample spinning rate of 14 kHz. ^{29}Si CPMAS NMR (CP contact time of 2 ms) and ^{29}Si MAS NMR spectra (after a 4 μs-90° pulse) were acquired with application of a strong ^1H decoupling pulse at 8 kHz of sample spinning. The recycle-delay time for the Bloch decay was 300 s. External references were used to calibrate the NMR shifts, and spectra were reported with reference to tetramethylsilane (TMS) for ^{29}Si nuclei, BF_3–$O(CH_2CH_3)_2$ for ^{11}B, and 1 N $Al(NO_3)_3$ aqueous solution for ^{27}Al nucleus. Pyridine chemisorption experiments were performed on a TG instrument 2920. Approximately 30 mg of sample (H-form) was heated to 550 °C in 100 mL/min of a dry N_2 flow, followed by a soak at this temperature for 3 h. After cooling to 150 °C, approximately 50 μL of pyridine was injected to the inlet line via syringe, and the system remained at 150 °C for 50 h. Acridine adsorption was performed at room temperature according to the following procedure. Approximately 3.0 mg of sample was placed in a 20 mL vial and dried at 175 °C in an oven for 4 h. After cooling, 2 mL of 500 μmol/L of acridine in hexane solution was added to the vial with a pipet (Eppendorf). The H-form zeolite sample immediately turned green upon addition of acridine. The mixture was slightly agitated by hand, and was allowed to rest in place for 30 min. The mixture was subsequently filtered with a 0.2 μm syringe filter to remove solids, and the filtrate was analyzed via UV–vis spectrometry. The amount of adsorbed acridine was calculated on the basis of disappearance of acridine from solution, which was measured by comparing the absorption at 355 nm before and after titration. Infrared spectra of self-supported zeolite pellets were recorded with a Nicolet 6700 FTIR spectrometer using 2 cm^{-1} resolution. For characterization of hydroxyl groups and adsorbed pyridine (Py), zeolite pellets were first activated at 500 °C in vacuo for 2 h. The background spectrum, recorded under identical operating conditions in the absence of a sample in the cell, was always automatically subtracted from measured spectra. For studying acid sites, the zeolite pellets were exposed to pyridine vapors for approximately 5 min at 25 °C. Spectra were recorded after evacuation for 1 h at 150 °C (3 °C/min ramp rate from 25 °C). The concentrations of the Brønsted and Lewis acid sites were calculated from the integrated area of PyH$^+$ and PyL infrared bands (at 1545 and 1456 cm^{-1}, respectively) using literature molar extinction coefficients of these bands (1.13 and 1.28 cm μmol^{-1}, respectively).[41]

Catalysis. All chemicals were purchased from Sigma-Aldrich Co. Acetic anhydride (Ac$_2$O) was further purified by refluxing over Mg granules for 5 days, followed by distillation, and then stored with activated 4Å molecular sieves before use. Acylation reactions were conducted in sealed, 48 mL thick-walled glass tubes equipped with a magnetic stirrer (600 rpm) and heated under autogenous pressure in
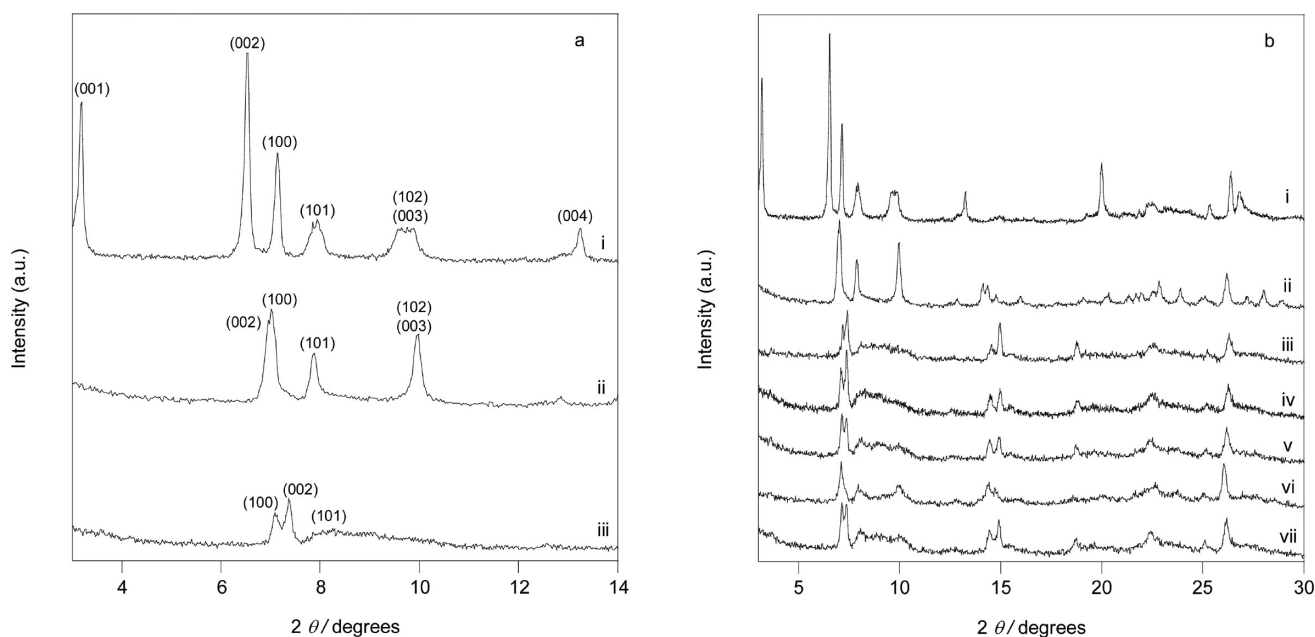
Figure 2. (a) PXRD patterns in $2\theta = 3-14°$ exhibiting reflection positions, as obtained from whole-pattern profile-fitting, for materials (i) ERB-1P, (ii) ERB-1C, and (iii) ERB-1-del-135. (b) PXRD patterns in $2\theta = 3-30°$ characterizing (i) ERB-1P, (ii) ERB-1C, (iii) ERB-1-del-100, (iv) ERB-1-del-135, (v) ERB-1-del-150, (vi) ERB-1-del-175, and (vii) ERB-1-del-135-D.

an oil bath at 120 °C, using Ac_2O as the acylating reagent and 1,2-dichloroethane as the solvent. Prior to use, 0.10 g of catalyst was activated in air at 500 °C. In 10 mL of 1,2-dichloroethane were dissolved 1.1 mmol of 2MN, 1.1 mmol of Ac_2O, and an internal standard (1.1 mmol of dodecane), and this mixture was added to the vessel. Aliquots from the reaction mixture were sampled and analyzed by gas chromatography (FID detector) using an Agilent 6890 and a 30-m HP-1 column. The products were identified by comparing their retention time relative to 2,6-AMN and 1,2-AMN.

■ RESULTS AND DISCUSSION

PXRD Characterization. The as-made precursor, calcined, and delaminated ERB-1 materials are denoted as ERB-1P, ERB-1C, and ERB-1-del-135, respectively, where 135 denotes the delamination temperature (°C). The PXRD data of ERB-1P, ERB-1C, and ERB-1-del-135 were analyzed using whole-pattern profile-fitting[34,35] ($2\theta = 3-30°$) (Figures S1–S3 in Supporting Information [SI]). The patterns of ERB-1P, ERB-1C, and ERB-1-del-135 are indexed on the basis of primitive hexagonal unit cells, as shown in Figure 2a. The unit cell parameters are summarized in Table 1. Low-angle peaks at 3.19° (reflection

Table 1. Unit Cell Parameters of As-Made, Calcined, and Delaminated ERB-1 Materials

sample	treatment	a (Å)	b (Å)
ERB-1P	as-made and air-dried	14.29	26.99
ERB-1C	directly calcined at 550 °C	14.06	24.76
ERB-1-del-135	delaminated in $Al(NO_3)_3$ solution at 135 °C, and calcined at 550 °C	14.11	23.53

(001)) and 6.55° (reflection (002)) represent the lamellar structure of ERB-1P. Peaks at 7.16° (reflection (100)), and 7.95° (reflection (101)) in pattern (i) in Figure 2a are consistent with those previously reported for ERB-1P.[31] Similar to previous observations by Millini et al., the intensities of the (001) and (002) reflections decrease significantly after calcination of ERB-1P at 550 °C in pattern (ii) in Figure 2a,
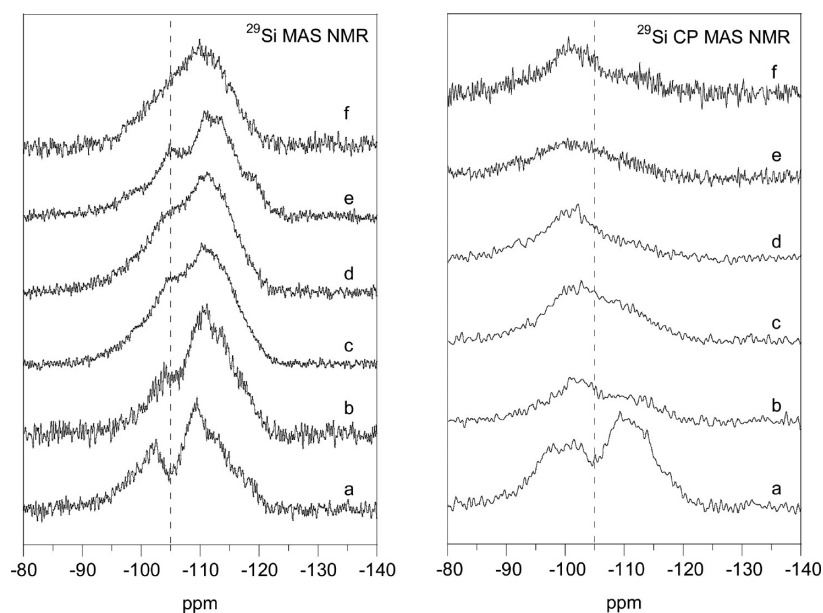
which is attributed to the formation of 10-MR structures between layers, along the c-axis.[31] Reflection (002) shifted from 6.55° in ERB-1P to a value of about 6.97° for ERB-1C, and merged with reflection (100) at 7.08°, so as to make a slightly split peak centered at around 7.04° for ERB-1C in pattern (ii) in Figure 2a. Such a shift in the (002) reflection corresponds to a significant contraction of the unit cell, from 26.99 Å in ERB-1P to 24.76 Å in ERB-1C along the c-axis, as shown in Table 1. A contraction along the a-axis from 14.29 Å in ERB-1P to 14.06 Å in ERB-1C is also observed. Both of these contractions are probably caused by the loss of the organic pore filler, PI, during calcination.

Delamination of ERB-1P using our approach consisting of isomorphous substitution of Al into the ERB-1 framework, followed by calcination, causes loss of long-range order along the c-axis and pronounced structural changes in the a-b plane. This is shown by comparing pattern (iii) in Figure 2a for ERB-1-del-135 with that of the calcined material ERB-1C. The (001) reflection for ERB-1-del-135 is too weak to be identified, as in ERB-1C. The (002) reflection shifted from 6.97° in ERB-1C to 7.39° in ERB-1-del-135 in Figure 2. Whole-pattern profile-fitting demonstrated a contraction of the unit cell along the c-axis, from 24.76 Å to 23.53 Å, and a unit cell expansion of 0.06 Å along the a-axis accompanying delamination, when comparing ERB-1-del-135 and ERB-1C. The latter expansion is likely caused by the isomorphous substitution of larger Al for smaller B atoms within the framework. Furthermore, the (100) reflection for ERB-1-del-135 also exhibits a small but important shift to lower 2θ angles relative to that for ERB-1C in Figure 2.

The sharp peaks for the (101) and (102) reflections in both ERB-1P and ERB-1C are no longer observed in ERB-1-del-135, as shown in pattern (iii) in Figure 2a. Instead, a broad band between 8° and 11° due to overlapping (101) and (102) reflections is clearly observed, and the relative intensity of this broad band has been previously used as a metric for evaluating the extent of delamination.[42] In patterns (iii, vi) in Figure 2b, the (101) and (102) reflections in the delaminated ERB-1

Figure 3. ^{29}Si MAS and ^{29}Si CPMAS NMR data characterizing (a) ERB-1C, (b) ERB-1-del-100, (c) ERB-1-del-135, (d) ERB-1-del-150, (e) ERB-1-del-175, and (f) ERB-1-del-135-D.

prepared at various temperatures are much lower in intensity compared with patterns (i) and (ii) for ERB-1P and ERB-1C, respectively, in Figure 2b. This is consistent with a lack of layer alignment in the delaminated ERB-1 materials, which are synthesized using our approach. In addition, on the basis of this data, ERB-1-del-135 (pattern (iv) in Figure 2b) is expected to have poorer layer-to-layer alignment than ERB-1-del-175 (pattern (vi) in Figure 2b). The partially dealuminated sample, ERB-1-del-135D (pattern (vii) in Figure 2b), shows a very similar reflection pattern compared to its parent sample, ERB-1-del-135, which suggests that the dealumination treatment consisting of acid leaching of extra-framework Al species does not lead to amorphization. This is supported by further characterization data below.

Solid-State NMR Spectroscopy. ^{29}Si MAS and CPMAS NMR spectra shown in Figure 3 characterize local structure in the same ERB-1-related materials as described above, within the context of Figure 2. All spectra in Figure 3 show the absence of a Q^2 ($\equiv(SiO)_2Si(OH)_2$) resonance, which would otherwise be expected to appear at approximately −80 ppm to −90 ppm.[43] This is strong corroborating evidence that there is no amorphization of the zeolite framework accompanying delamination during our treatment procedure. The resonances in all materials are overall broad, and this is consistent with the low silicon relative to heteroatom content of all materials (i.e., the low Si/B ratio of the parent ERB-1(P) sample). A comparison of the ^{29}Si MAS and ^{29}Si CPMAS spectra for each sample demonstrates the presence of silanol-related resonances (i.e., the −101 ppm resonance representing Q^3 ($\equiv(SiO)_3\mathbf{Si}OH$) Si atoms is stronger than resonances centered around −105 ppm representing Q^4 ($\equiv(SiO)_4Si$) Si atoms in the CPMAS spectrum, which is opposite the observed relative intensity trend in the MAS spectrum). The specific assignments of Q^3 and Q^4 resonances are consistent with results previously reported by Camblor et al. for ITQ-1 material[44,45] and are as follows: −94.8 ppm (Q^3), −100.9 ppm (Q^3), −105.2 ppm (Q^4), −110.3 ppm (Q^4), −113.1 ppm (Q^4), −116.5 ppm (Q^4), and −119.5 ppm (Q^4). We conducted spectral fitting of the ^{29}Si MAS spectra, and on the basis of these fits, we calculated the

Q^3/Q^4 ratios in order to evaluate the extent of delamination (Figure S4, SI). Our expectation is that greater delamination results in a higher Q^3/Q^4 ratio as a result of fewer 10-MR formed due to condensation between layers. All delaminated ERB-1 materials synthesized using our approach show a higher Q^3/Q^4 ratio compared with ERB-1C, and ERB-1-del-135 exhibits the highest Q^3/Q^4 ratio relative to ERB-1-del-100 and ERB-1-del-175. This suggests that treatment at 135 °C using our approach leads to a greater extent of layer separation than at either 100 or 175 °C. The ^{29}Si MAS and CPMAS NMR spectra of the partially dealuminated sample that was delaminated at 135 °C, ERB-1-del-135D (Si/Al = 44, Si/B > 200) in Figure 3f, is very similar to the parent material before dealumination consisting of ERB-1-del-135. Therefore, the dealumination treatment has virtually almost no effect on crystallinity, which is consistent with the PXRD analysis above.

^{11}B MAS NMR spectra of the as-made, directly calcined, and delaminated ERB-1 materials are shown in Figure 4. ^{11}B MAS NMR resonances that are narrowly clustered in the range of −5 to 0 ppm are typically assigned to tetrahedrally coordinated boron sites ($B[4]$) within framework T positions.[29] Broadened resonances between 0 and 20 ppm are generally assigned to trigonally coordinated boron sites ($B[3]$), and very broad line shapes downfield (10−17 ppm) are typically assigned to extra-framework $B[3]$ species, which do not contain B−O−Si bonds (such as $B(OH)_3$).[29,46,47] The spectrum of ERB-1P in Figure 4a has at least three major overlapping resonances (centered at −2.0 ppm, −3.2 ppm, and −3.9 ppm, respectively), which can all be assigned to tetrahedrally coordinated $B[4]$ sites, and there is no evidence of $B[3]$ sites in the ERB-1P material according to data in Figure 4a.

The ^{11}B MAS NMR spectrum of the calcined precursor, consisting of ERB-1C (Si/B = 10) in Figure 4b, has different distributions of $B[4]$ sites relative to ERB-1P. Resonances at −2.0 and −3.9 ppm are diminished in intensity significantly, and there are two new broad resonances centered at 7.5 and 15 ppm, respectively, which emerged due to possible formation of framework $B[3]$ sites and extra-framework $B[3]$ sites, respectively.[29] The formation of framework $B[3]$ sites may be
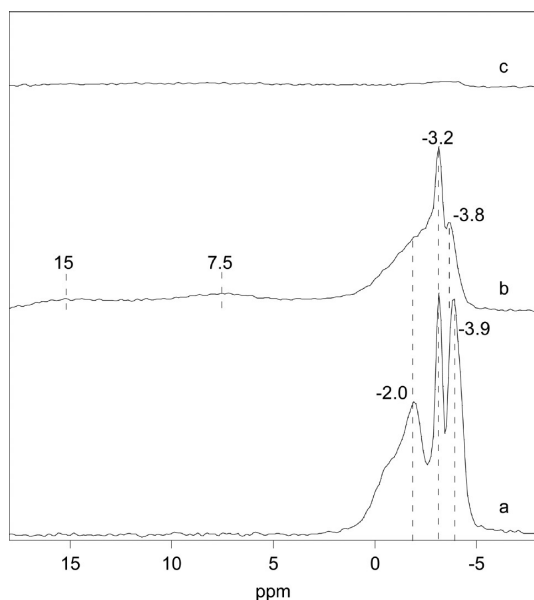
Figure 4. ^{11}B MAS NMR data characterizing (a) ERB-1P, (b) ERB-1C, (c) ERB-1-del-135.

Figure 5. ^{27}Al MAS NMR data characterizing (a) ERB-1-del-135-D, (b) ERB-1-del-100, (c) ERB-1-del-135, and (d) ERB-1-del-175.

due to either (i) the dehydration of water-coordinated B[4] sites according to $(SiO)_3B{:}OH_2 \rightarrow (SiO)_3B + H_2O$ or (ii) decoordination of PI that is originally attached to B[4] species according to $(SiO)_3B{:}PI \rightarrow (SiO_3)B + PI$ during calcination. The possible emergence of some extra-framework B[3] sites in ERB-1C may be due to some deboronation via hydrolysis during calcination of ERB-1P.

The lack of an observable B resonance in the ^{11}B MAS NMR spectrum of ERB-1-del-135 in Figure 4c suggests that our delamination approach removes virtually all B present in the precursor stage of the material. This is likely brought about by the mildly acidic $Al(NO_3)_3$ solution (pH ≈ 3) that has been used for delamination and is consistent with the high Si/B ratios, as measured by elemental analysis and reported in Table 2.

^{27}Al MAS NMR spectra of delaminated and partially dealuminated and delaminated ERB-1 materials are shown in Figure 5. The ^{27}Al MAS NMR resonance at 52 ppm is generally assigned to a framework tetrahedrally coordinated Al species (Al[4]),[48] whereas the resonance at around 0 ppm is typically assigned to extra-framework Al[6] sites.[49,50] Elemental analysis results, which are summarized in Table 2, show that ERB-1-del-100 (Si/Al = 18) and ERB-1-del-135 (Si/Al =15) partially
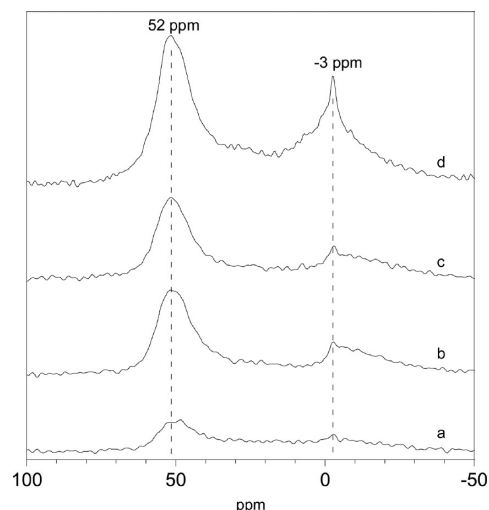
substitute lattice Al for B. Such a result of partial isomorphous substitution is consistent with expectations based on Al being able to reinsert for B into 12-MR surface pockets, and Al being unable to do this in a 10-MR. This has been previously shown by Chen et al. and is attributed to the large size of the hydrated $Al(H_2O)_6^{3+}$ cation, which is unable to access 10-MR channels.[23] Both materials ERB-1-del-100 and ERB-1-del-135 (Figures 5b,c) show that about 75% of the Al sites are tetrahedrally coordinated species (AlO_4), and about 25% of them are extra-framework octahedrally coordinated species (AlO_6). Interestingly, ERB-1-del-175, which consists of the greatest amount of Al reinsertion and where the Si/Al = 10 is even lower than the Si/B = 11 of the parent ERB-1P precursor material, has a very strong band centered at −3 ppm due to the extra-framework Al[6] resonance in Figure 5d. This indicates that many of the Al sites in ERB-1-del-175 are located in extra-framework positions, which is probably because at such a high temperature (as opposed to 100 °C as used by Chen et al.[23]), dealumination is probably competing with Al reinsertion. Finally, both elemental analysis (Si/Al = 44) in Table 2 and the ^{27}Al MAS NMR spectrum of the partially dealuminated ERB-1-del-135D in Figure 5a show a reduction of overall aluminum content relative to ERB-1-del-135 and a nearly complete elimination of extra-framework Al[6] species after acid treatment.

TEM Characterization. TEM images of ERB-1P show the expected lamellar assembly consisting of rectilinear sheets

Table 2. Results from Chemical Analysis of As-Made Materials and Nitrogen Physisorption Measurement of Calcined Materials

sample	Si/B ratio	Si/Al ratio	$V_{micro}{}^a$ (cm^3/g)	$V_{meso}{}^b$ (cm^3/g)	$S_{ext}{}^c$ (m^2/g)	uptake of acridine^d (μmol/g)
ERB-1P	11	n/a	n/a	n/a	n/a	0
ERB-1C	10	n/a	0.12	0.04	53	0
ERB-1C-Al	>200	135	0.12	0.04	54	59
ERB-1-del-100	>200	18	0.11	0.05	71	164
ERB-1-del-135	>200	15	0.09	0.08	133	168
ERB-1-del-150	>200	16	0.06	0.08	129	122
ERB-1-del-175	>200	10	0.08	0.03	30	47
ERB-1-del-135D	>200	44	0.09	0.08	125	108
H-MCM-22	n/a	40	0.14	0.04	56	80

^{a}Micropore volume determined by t-plot method. ^{b}Mesopore (between 1 and 10 nm in diameter) volume determined by NLDFT method. ^{c}External surface area. ^{d}The titration of acridine was conducted at room temperature. Three mg of zeolite sample was treated with 2 mL of 500 μmol/L acridine/hexane solution. The disappearance of acridine was checked by liquid phase UV−vis spectroscopy.
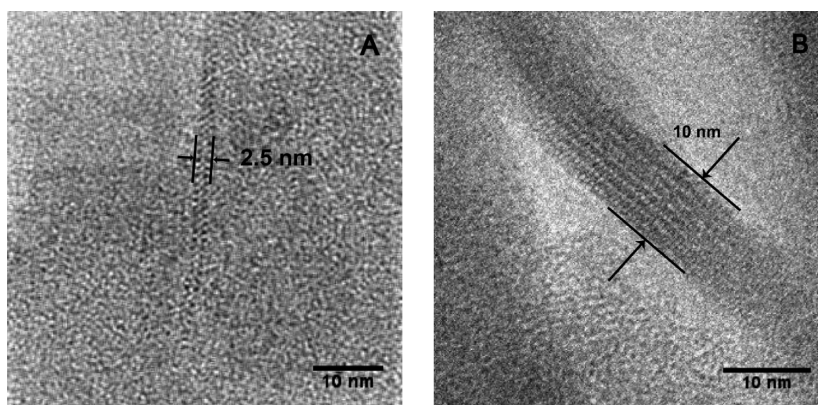
Figure 6. TEM images characterizing ERB-1-del-135. The arrows indicate single-layers (A) and four-layers (B).

(Figure S5 in SI), whereas in comparison images of the delaminated zeolite ERB-1-del-135 in Figure 2 clearly show curved thin layers, which lack long-range order, which is consistent with PXRD data in Figure 2. A representative single layer of 2.5 nm thickness, and a four-layer assembly of 10 nm thickness are shown in A and B of Figure 6, respectively.

N_2 Physisorption at 77 K. N_2 adsorption−desorption isotherms of ERB-1C and ERB-1-del-135 were measured for textural characterization and are shown in Figure 7, and the
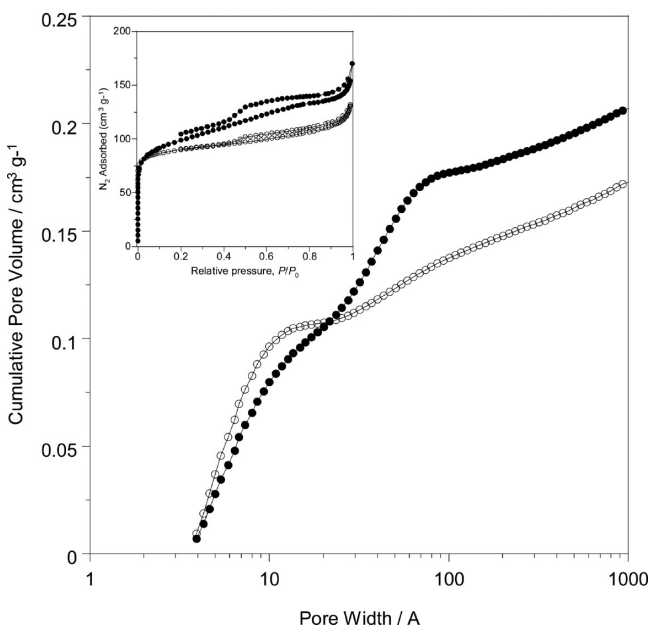

Figure 7. N_2 NLDFT cumulative pore volume plots for (○) ERB-1C and (●) ERB-1-del-135. The inset shows the corresponding N_2 adsorption isotherms.

pore size distributions derived from the NLDFT model[40] are illustrated in Figure S6, SI. Table 2 lists micropore and mesopore volumes, as well as external surface areas, as determined by the *t*-plot method. The partially dealuminated ERB-1-del-135 (Si/Al = 15, Si/B > 200), denoted as ERB-1-del-135D (Si/Al= 44, Si/B > 200), still has almost the same micropore and mesopore volume as well as external surface area (0.09 cm^3/g, 0.08 cm^3/g, and 125 m^2/g, respectively) as its parent material ERB-1-del-135, which further reinforces PXRD and solid-state NMR data that the dealumination by acid treatment does not amorphize the zeolite framework. The

external surface area of ERB-1-del-135D is 2.7-fold higher than that of the corresponding calcined 3D zeolites ERB-1C and ERB-1C-Al. ERB-1C-Al (Si/Al = 135, Si/B > 200) is prepared from the Al-exchanged ERB-1C where the B in the 12-MR surface pockets of ERB-1C is substituted by Al. Indeed, ERB-1-del-135 and ERB-1-del-150 both exhibit significantly lower micropore volume, higher mesopore volume, and higher external surface areas, relative to the corresponding calcined 3D zeolites, ERB-1C and ERB-1C-Al. On the other hand, ERB-1-del-100 does not show as much micropore, mesopore volume, and external surface area, consistent with its lack of delamination as discussed and shown using other methods above. Interestingly, material ERB-1-del-175 shows significantly smaller micropore volume (0.08 cm^3/g vs 0.12 cm^3/g for ERB-1C) when compared with the corresponding calcined 3D zeolite, but its external surface area is slightly lower than that of the 3D zeolite. We attribute this reduction in micropore volume to pore blockage by the large amount of extra-framework Al[6] species, as evidenced by ^{27}Al MAS NMR spectroscopy, rather than a high degree of delamination. Therefore, it is clear that the high efficiency of delamination of ERB-1P by isomorphous substitution of Al for B must be conducted within a properly controlled temperature, which is rather narrowly defined within a preferable range around 135 °C.

Base Titration of Acid Sites. To quantify the relative number density of external-surface acid sites, we developed acridine titration in the liquid phase as a rapid method that allows screening and comparison of different materials. The titration of acid sites by acridine is illustrated in Scheme 1. We observe a color change of the acridine from colorless in solution to green upon adsorption. Such a distinct color change is consistent with acridine protonation upon adsorption to the acid site.[51] Acridine is structurally related to anthracene with

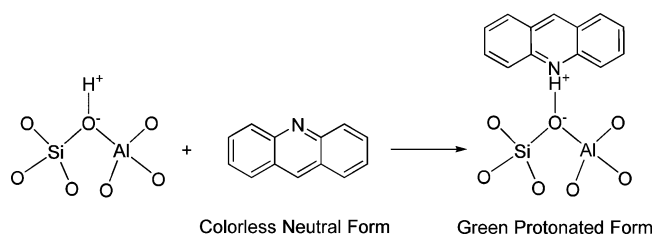**Scheme 1. Titration of Brønsted Acid Sites by Acridine in Hexane Solution**

Colorless Neutral Form   Green Protonated Form

Table 3. Temperature Desorption Profile of Pyridine Chemisorbed onto Zeolites at 150 °C

| | | | | fraction of pyridine adsorbed at 150 °C retained at higher temperature[a] | | |
samples	Si/Al	uptake of pyridine at 150 °C (μmol/g)	acridine/pyridine ratio	200 °C (%)	250 °C (%)	350 °C (%)
ERB-1-del-135	15	278	1.65	69.5	48.8	17.3
ERB-1-del-135D	44	106	0.98	73.4	48.2	21.1

[a]The fraction is calculated by dividing the total acid sites by the amount of chemisorbed pyridine retained at certain temperatures.

one of the central CH groups replaced by a basic nitrogen atom. The acidity of the conjugate acid of acridine is moderate with a pK_a of 5.6, making acridine a weak base that is comparable to pyridine, which itself is commonly used as a probe of internal-pore acid sites in materials.[52,53] This weak base strength of acridine is advantageous from the perspective of avoiding adventitious adsorption on silanol groups, and such a lack of silanol adsorption of acridine can be experimentally verified using Aerosil 200 (Evonik Industries) in hexane solution at room temperature. Acridine does not adsorb to Aerosil 200, whereas pyridine adsorbs significantly under the same conditions (using 2 mL of a 500 mM solution of base in hexane and 3 mg of Aerosil 200).

Acridine adsorption is used as a contributing metric for evaluating the extent of layered zeolite precursor delamination. Acridine titration data of various delaminated and partially dealuminated and delaminated materials are summarized in Table 2. ERB-1P and ERB-1C exhibit a lack of acridine uptake presumably because the acidity of tetrahedral B sites is too weak and not all that far removed from the silanol acidity described above. ERB-1C-Al (Si/Al = 135) is a 3D zeolite that has postsynthetic isomorphous substitution of Al for B. As mentioned above, because such substitution cannot occur through 10-MR channels, this postsynthetic treatment is expected to work for only external-surface framework Al sites. The acridine titration data below demonstrate that such a hypothesis is correct. The measured acridine uptake for ERB-1C-Al is 59 μmol/g. H-MCM-22 (Si/Al = 40) has a much higher bulk density of Al sites compared with ERB-1C-Al; however, it has almost the same amount of acridine adsorption. This last result is consistent and emphasizes the external-surface nature of acridine adsorption in all experiments described here, which is consistent with its inability to enter 10-MR due to steric constraints, and also emphasizes the inability to perform postsynthetic isomorphous substitution of Al for B through 10-MR channels.

Data in Table 2 indicate that ERB-1-del-135 has the highest density of external acid sites based on acridine uptake, which is 2.2-fold higher than for ERB-1C-Al, and is consistent with the fact that this material also shows the largest measured external surface area of all materials. The acid-site strength of the delaminated ERB-1-del-135 material as well as its partially dealuminated ERB-1-del-135D counterpart material was investigated by pyridine adsorption at 150 °C followed by desorption at 200 °C, 250 °C, and 350 °C. The amount of pyridine adsorbed at each temperature was measured gravimetrically and was used to determine the density of acid sites. These results are summarized in Table 3. At 150 °C, the density of chemisorbed pyridine on ERB-1-del-135 and ERB-1-del-135D is 278 and 102 μmol/g, respectively, corresponding to 69.5 and 73.4% of their total acid-site density (calculated on the basis of Si/Al ratio). After partial dealumination to remove octahedral extra-framework Al and decrease average proximity between Al sites, ERB-1-del-135D (21.1% pyridine remaining

at 350 °C) shows on average stronger acid strength compared to ERB-1-del-135 (17.3% pyridine remaining at 350 °C).

FTIR Spectroscopic Characterization. FTIR spectroscopy was used to characterize hydroxyl groups in various materials, and infrared spectra (normalized with respect to weight) of 3D and delaminated ERB-1 materials are shown in Figure 8. The band at 3747 cm^{-1} is due to non-interacting
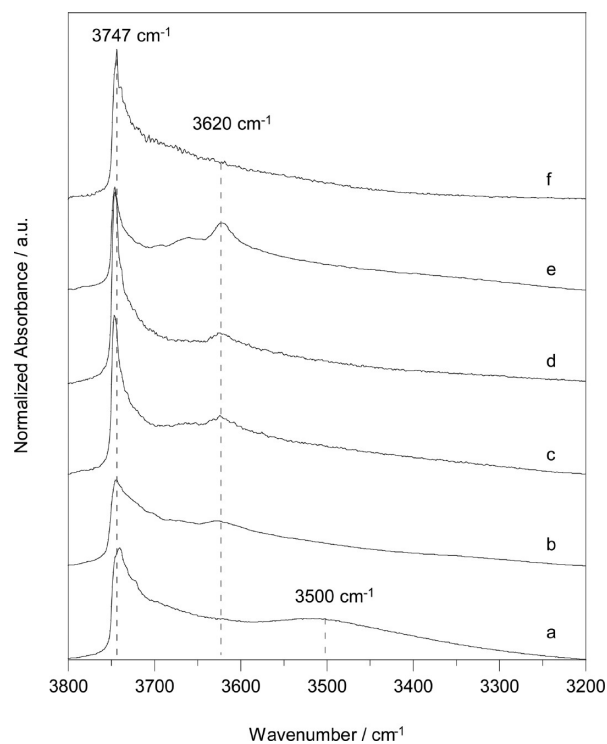

Figure 8. FTIR spectra of ERB-1 related materials. (a) ERB-1C-Al, (b) ERB-1-del-100, (c) ERB-1-del-135, (d) ERB-1-del-150, (e) ERB-1-del-175, and (f) ERB-1-del-135D.

silanols (no H-bonding between silanols).[54] Delamination in principle avoids formation of 10-MR between layers by preventing interlayer silanol condensation; therefore, a higher density of noninteracting SiOH species is expected to be present after delamination.[55] ERB-1-del-135 (Figure 8c) and ERB-1-del-150 (Figure 8d) show a greater intensity and a sharper band at 3747 cm^{-1} than the 3D zeolite and the delaminated ERB-1 at other temperatures, such as 100 and 175 °C. This corroborates data from ^{29}Si MAS NMR spectroscopy, N$_2$ physisorption, PXRD, and acridine adsorption above, and suggests that delamination at 135 °C is optimal and leads to the greatest extent of exfoliation in our current investigation. The infrared spectrum of the partially dealuminated and delaminated material ERB-1-del-135D (Figure 8f) still shows a sharp band located at 3747 cm^{-1}. This suggests that the high external-surface area is intact after acid treatment and supports data

from PXRD, ^{29}Si MAS NMR spectroscopy, and N$_2$ physisorption. Some intensity at lower infrared frequency at ~3730 cm^{-1} was observed in the spectra for all materials. Such an infrared band (3730 cm^{-1}) has been previously assigned to silanol groups located near structural defects, or silanol nests, on the internal surface.[56] The high Si/Al materials, i.e., ERB-1C-Al, ERB-1-del-100, and ERB-1-del-135D, are expected to consist of a higher density of silanol nests. This is consistent with a more prominent stretching band at ~3730 cm^{-1} than materials, such as ERB-1-del-135, which consist of lower Si/Al ratios.

The infrared band at 3620 cm^{-1} is due to Brønsted acid sites, Si(OH)Al.[57] The presence of the band at 3620 cm^{-1} confirms the success in isomorphous substitution of Al for B, since B sites alone do not exhibit such a band. ERB-1-del-135 and ERB-1-del-150 both have clear bands at 3620 cm^{-1}, which confirms the success in synthesizing strong Al-Brønsted acid sites within a tetrahedral coordination environment in these materials. ERB-1-del-175 (Figure 8e) consisting of a low Si/Al of 10 shows the strongest band at 3620 cm^{-1} among all delaminated samples. Interestingly, ERB-1-del-175 also has a strong absorption band at 3720 − 3640 cm^{-1}, which has been previously assigned to OH groups on extra-framework Al and/ or on tetrahedrally connected Al that has been partially hydrolyzed from the framework.[58,59] This is consistent with the presence of the strong resonance at around 0 ppm for octahedral Al via ^{27}Al MAS NMR spectroscopy. The spectrum of ERB-1C-Al (Figure 8a) does not show an appreciable band at 3620 cm^{-1}, indicating a low density of Brønsted acid sites (Si/Al = 135); instead, it has strong infrared bands at ~3730 and 3500 cm^{-1} due to internal silanol groups from either structural defects or silanol nests.[57] Similarly, the partially dealuminated sample, ERB-1-del-135D, also does not show appreciable bands at 3620 cm^{-1} and exhibits intensity that is so low that it is overlapped with other bands.

FTIR spectroscopy was also performed on samples consisting of adsorbed pyridine in order to estimate and differentiate between Brønsted and Lewis acid sites. The amount and strength of Brønsted and Lewis acid sites of the delaminated sample, ERB-1-del-135, and the partially dealuminated sample, ERB-1-del-135D, were compared by first adsorbing pyridine at 25 °C and subsequently desorbing at 150 °C. The infrared spectra obtained after pyridine desorption at 150 °C are shown in Figure 9 for the window spanning 1440−1700 cm^{-1}. A usual set of bands was observed: two bands at 1542 cm^{-1} and 1637 cm^{-1}, which are generally assigned to pyridinium ion (PyH$^+$), two bands at 1453 cm^{-1} and 1621 cm^{-1}, which are typically assigned to Lewis-acid sites coordinated to pyridine (PyL), and a band at 1490 cm^{-1}, which has been previously described as the superposition of signals of both PyH$^+$ and PyL species.[60] The dealumination treatment of the delaminated material causes a decrease in the intensity of bands corresponding to pyridine adsorbed on both Brønsted and Lewis acid sites, which is consistent with the ^{27}Al MAS NMR spectroscopic results, which also show a decrease in overall acid-site content. The ratio between the Brønsted acid sites and Lewis acid sites increases from 1.9 to 4.3 after dealumination (Table S1, SI). This suggests that the Lewis acid sites are more labile during acid treatment relative to Brønsted acid sites.

Comparative Synthetic Studies of Delamination. We conducted several comparative synthetic studies in order to more fully understand the crucial features that are responsible
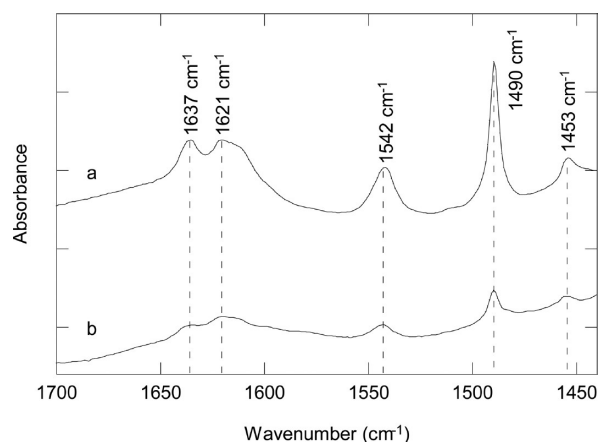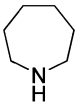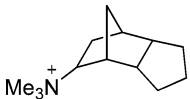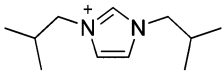

Figure 9. FTIR spectra of activated samples, (a) ERB-1-del-135 and (b) ERB-1-del-135D, recorded after pyridine adsorption at 25 °C and desorption at 150 °C.

for delaminating layered borosilicate zeolite precursors when using our method of isomorphous substitution. First, we consider that there are two roles of Al(NO$_3$)$_3$ treatment for effecting delamination. The first of these is that aqueous Al(NO$_3$)$_3$ solution contains bulky hydrated Al(H$_2$O)$_6^{3+}$ cations, which disrupt the interlayer hydrogen bonding before getting close enough to occupy silanol nests and complete framework insertion. Second, the Al(NO$_3$)$_3$ solution is mildly acidic, at pH ≈ 3, which contributes to PI organic template and framework B removal[61] via its leaching (Figures S7 and S8, SI). These two phenomena may have a synergistic effect on delamination, and B removal in particular may also disrupt interlayer hydrogen bonding. To explore the necessity of the Al(H$_2$O)$_6^{3+}$ cation on delamination, we treated ERB-1P in acids only, such as dilute HNO$_3$ solution (pH = 3) either at 135 °C or room temperature, as well as 50 wt % acetic acid (pH = 1.5) at 135 °C. As summarized in Table 4, none of these Al-free conditions show any success in delamination. Instead, there is even a slight decrease in micropore volume and external surface area, probably due to partial collapse of the zeolite structure caused by the loss of framework B without replenishment with other heteroatoms in the T positions, when performing these acid-only treatments. Therefore, Al(H$_2$O)$_6^{3+}$ and H$_3$O$^+$ both have important roles in our delamination approach.

Next, we attempted delamination with Al(NO$_3$)$_3$ solution on several other layered zeolite precursors and silicates, including MCM-22P,[62] Na-kanemite,[63] B-SSZ-25,[32] and B-SSZ-70.[33,64] We considered two factors when choosing these reference materials. First, we investigated the importance of whether the presence of B in the zeolite framework is crucial to delamination. Second, we chose materials so as to vary the role of the organics, which can be either as a pore filler when used as a small neutral amine or as a structure-directing agent when used as a bulky quaternary SDA. MCM-22P does not have any B in its framework, but it has HMI as the pore filler, which is very similar to the role of PI in ERB-1P. Thus, this comparison can be used to inform whether B is necessary for delamination. On the other hand, B-SSZ-25 and B-SSZ-70 both have B in their framework, but the organic template is a bulky quaternary ammonium salt consisting of a SDA. Therefore, a comparison of ERB-1P with B-SSZ-25 and B-SSZ-70 was used to better understand the role of the organics in delamination.

1457

dx.doi.org/10.1021/ja410141u | J. Am. Chem. Soc. 2014, 136, 1449−1461

Table 4. Comparative Studies of Delamination^a of Various Layered Zeolite Precursors

samples	SDA	reagent	Si/Al ratio	Si/B ratio	3D zeolite V_{micro} (cm^3/g)	3D zeolite S_{ext}^b (m^2/g)	After delamination V_{micro} (cm^3/g)	After delamination S_{ext}^b (m^2/g)
ERB-1P	(piperidine)	Al(NO$_3$)$_3$	15	n/a			0.09	133
		HNO$_3$ ^{c}			0.12	53	0.06	13
		HNO$_3$ (r.t.) ^{d}	n/a	11			0.15	25
		HAc ^{e}					0.10	20
MCM-22P	(azepane)	Al(NO$_3$)$_3$	27	n/a	0.14	56	0.12	55
Na-kanemite	n/a	Al(NO$_3$)$_3$	n/a	n/a	0	6	0	6
B-SSZ-25	(Me$_3$N$^+$)	Al(NO$_3$)$_3$ ^{f}	n/a	35	0.13	30	0.11	23
B-SSZ-70	(imidazolium)	Al(NO$_3$)$_3$ ^{f}	n/a	30	0.18	54	0.18	55

^{a}The delamination was conducted on 200 mg of each zeolite precursor in 0.4 N Al(NO$_3$)$_3$ solution at 135 °C for 1 d. The resulting materials were calcined in air at 550 °C for 5 h to remove SDAs. ^{b}External surface area determined by t-plot method. ^{c}200 mg of ERB-1P was treated with HNO$_3$ solution, pH = 3, at 135 °C for 1 d, and then calcined in air at 550 °C for 5 h. ^{d}Same as footnote c, except that the treatment was conducted at room temperature for 1 d. ^{e}200 mg of ERB-1P was treated with 50 wt % HAc solution, pH = 1.5, at 135 °C for 1 d, and then calcined in air at 550 °C for 5 h. ^{f}The Al content is negligible (~200 ppm).

Finally, Na-kanemite was used because it has neither B nor organic templates.

Results of our attempts for delaminating the aforementioned layered zeolite precursors are listed in Table 4. There was no increase in external surface area for B-SSZ-25 and B-SSZ-70 after treating with Al(NO$_3$)$_3$ solution (Table 4). The SDAs for B-SSZ-25 and B-SSZ-70 syntheses were sterically bulky quaternized amines, and we found no removal of these SDAs upon attempting delamination under our conditions, when using TGA analysis. The possible reason may be that these SDAs are impossible to extract via protonation and remain too tightly bound inside of the zeolite cages due to their larger size. Thus, we believe that when using our method, a relatively small and neutral pore filler is also required for delamination. Although MCM-22P has a pore filler very similar to that of ERB-1P, its delamination with our method was also unsuccessful, evidenced by no increase in external surface area (Table 4). This result suggests that B is required in the layered zeolite precursor and that only removal of some organic SDA does not lead to delamination when using our method. The attempt to delaminate Na-Kanemite with our approach was also unsuccessful, which can be rationalized on the basis of lack of both framework B and organic template as pore filler.

Friedel–Crafts Acylation Catalysis. We used the Friedel−Crafts acylation (FCA) of 2MN with Ac$_2$O in the liquid phase as a model reaction to investigate the acid-catalysis properties of delaminated ERB-1 materials and compare them with 3D calcined zeolites. This reaction is shown in Scheme 2

Scheme 2. Chemical Equation of FCA of 2MN with A$_2$O
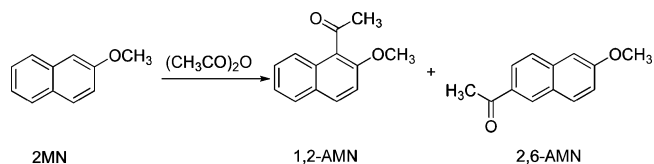
and was chosen because it provides direct information about external acid-site accessibility and catalytic activity, since the reaction should only occur on the external surface, due to the steric bulk of the reactants. This reaction has been used as the leadoff reaction in the first reported large-scale synthesis of the pain-reliever drug naproxen,[65] and has other applications in fine-chemicals synthesis. More broadly, FCA as a reaction class is relevant because it represents one of many examples where replacement of conventional homogeneous acid catalysts has

been successfully accomplished using recyclable and environmentally benign zeolite catalysts.[66,67]

The acylation of 2MN has been investigated over several molecular-sieve catalysts, such as H-MCM-41,[68] HY, H-ZSM-12, and *BEA.[69−71] Two products are typically observed consisting of 1-acetyl-2-methoxynaphthalene (1,2-AMN) and 2-acetyl-6-methoxynaphthalene (2,6-AMN), with the kinetically favored 1,2-AMN product usually predominating, often in yields of greater than 95%. Almost all previously reported solid-acid catalysts do not show selectivity for 2,6-AMN, except *BEA which has a 3D 12-MR channel system, and achieves ~50% selectivity for 2,6-AMN due to shape selectivity within its 12-MR channels.[69,71] Other products such as 2,8-AMN and diacylated products are not typically observed in the liquid phase and have only been observed in extracts of used solid catalysts.[71] We wished to use the acylation of 2MN using delaminated ERB-1 catalysts in order to specifically investigate the following: (i) how FCA activity is correlated with external acid-site density; (ii) how partial dealumination influences FCA activity due to the slightly enhanced acid strength relative to as-made delaminated materials, as observed above via pyridine adsorption and infrared spectroscopy; (iii) whether it is possible to observe evidence of shape-selectivity effects for 2,6-AMN, such as that which could be exhibited by external-surface 12-MR pockets via a nest effect.[72,73]

Catalysis data on the acylation of 2MN with Ac_2O over various catalysts is summarized in Table 5. The selectivities for

Table 5. Acylation of 2MN Catalyzed by ERB-1 Related Zeolites[a]

sample	conversion of 2MN (%)	yield (%) 1,2-AMN	2,6-AMN	selectivity (%) 1,2-AMN	2,6-AMN
ERB-1-del-100	14.5	13.9	0.6	95.7	4.3
ERB-1-del-135	20.4	19.4	0.9	95.7	4.3
ERB-1-del-150	16.1	15.2	0.8	95.2	4.8
ERB-1-del-175	13.5	8.6	0.4	95.5	4.5
ERB-1-del-135-D	41.2	38.2	1.8	95.4	4.6
ERB-1C-Al	18.0	17.1	0.8	95.6	4.4
H-beta[b]	38.7	18.4	18.3	50.1	49.9
H-MCM-22[c]	25.4	22.6	1.2	94.8	5.2
H-SSZ-70[d]	29.9	28.0	1.8	93.9	6.1

[a]Reaction condition: 100 mg of catalyst, Ac_2O: 2MN, 1:1 and 1.1 mmol, 10 mL of dichloroethane, 120 °C, 3 h. [b]Si/Al = 27. [c]Si/Al = 40. [d]Prepared from B-SSZ-70 via Al reinsertion, Si/Al = 130.

1,2-AMN over all catalysts except H-beta are all above or near 95%. The conversion of 2MN over delaminated ERB-1 catalysts follows the order: ERB-1-del-135 > ERB-1-del-150 > ERB-1-del-100 > ERB-1-del-175, which increases along the same trend as the external-surface area and uptake of acridine. When comparing observed 2MN conversions for ERB-1-del-135 (20.4%) and ERB-1C-Al (18.0%), delamination slightly improves conversion but less than the expected amount based on the 2.5-fold increase in external-surface area. Indeed, the FCA activities over most delaminated ERB-1 catalysts are not superior to their 3D counterpart, ERB-1C-Al, as well as other 3D zeolites listed in Table 5, despite the significantly higher density of accessible external-surface acid sites of the former, as measured above using acridine titration. We hypothesized that the lower-than-expected FCA activity may be due to the low Si/Al ratio of these delaminated materials,

since previous studies have revealed that higher Al impedes catalysis. For example, Davis et al. studied the effect of crystal size of H-beta on the acylation of 2MN. A small-crystal H-beta (Si/Al = 12, <1 μm) was found to have almost the same 2MN conversion as a large-crystal H-beta (Si/Al = 40, 2.5, and 9 μm).[71] Also, Moreau et al. reported that the acylation of 2MN over more acidic HY zeolite (Si/Al = 15) is much slower than a less acidic HY zeolite (Si/Al = 100), by a factor of 5-fold.[74] On the basis of these previously reported data, we hypothesized that the low Si/Al ratio may lead to a high Al density but low acid strength, with such a hypothesis being supported by our pyridine desorption and infrared spectroscopic data.

We performed dealumination on the most promising delaminated catalyst consisting of ERB-1-del-135 in order to partially remove extra-framework Al. Our rationale was that the stability and average acid strength of the remaining sites could be improved, due to the preferential loss of Al atoms that are proximal to each other, as reported previously.[75] Figure 10
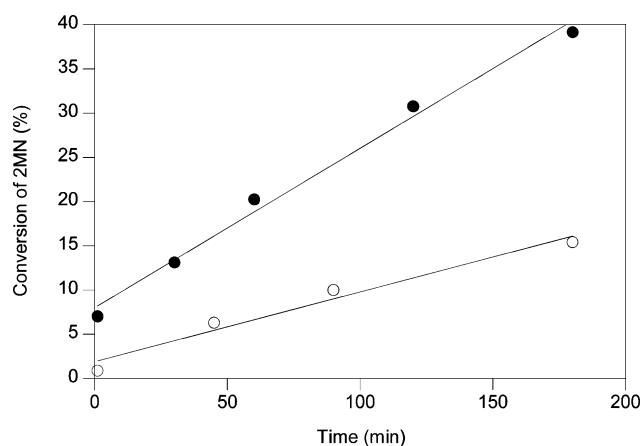

Figure 10. Catalysis kinetics of 2MN reacting with Ac_2O over ERB-1-del-135D (●) and ERB-1C-Al (○). The ratio of rates for catalysts ERB-1-del-135D to ERB-1C-Al is 2.3. (Reaction condition: 100 mg of catalyst, 120 °C, Ac_2O: 2MN, 1:1 and 1.1 mmol, 10 mL of dichloroethane.)

shows a comparison of the initial rates between the delaminated and partially dealuminated ERB-1-del-135D and its 3D counterpart ERB-1C-Al. The initial rate of catalysis (given by the slopes of the lines in Figure 10) when using ERB-1-del-135D is 2.3-fold higher than ERB-1C-Al. This is nearly equal to the 2.5-fold increase in external surface area due to delamination. Such a finding suggests that the catalysis rate for this FCA reaction proportionally scales with the density of external acid sites and is consistent with the size of the naphthalenic reactants relative to the zeolitic micropores. The more than 2-fold observed improvement in the catalytic activity of the partially dealuminated and delaminated ERB-1-del-135D relative to its nondealuminated counterpart ERB-1-del-135 is consistent with Al pairing being the reason for lower activity in the latter catalyst. Thus, dealumination via acid treatment is proposed to remove extra-framework Al that acts to hinder tetrahedral Al sites, presumably by coordinating to them.

■ CONCLUSIONS

We report herein a surfactant-free synthesis of delaminated MWW aluminosilicate zeolite, which is synthesized by heating a MWW borosilicate zeolite precursor, ERB-1P, in 0.4 M

aqueous aluminum nitrate solution. During this treatment, powder X-ray diffraction (PXRD) shows a complete loss of long-range order, and transmission electron microscopy (TEM) shows loss of rectilinear microstructure and formation of curved layers and some single layers. N_2 physisorption shows a consistent increase in external surface accompanying delamination, represented by a factor of up to 2.5-fold, and acridine titration shows a similar enhancement in the number density of external acid sites due to delamination. This external surface-area increase is also consistent with the increased Q^3/Q^4 ratio as measured by ^{29}Si NMR spectroscopy when comparing the delaminated versus 3D calcined ERB-1C materials, since some interlayer 10-MR systems in the latter are replaced by silanols in the former. Comparative synthetic studies of the delamination process employing related MWW layered zeolite precursors demonstrate that both framework B and a neutral pore filler (rather than a quaternary ammonium structure-directing agent) are required. The delamination of ERB-1P occurs with isomorphous substitution of tetrahedral aluminum for boron, as evidenced by ^{11}B and ^{27}Al NMR spectroscopies, with the delaminated materials consisting of Brønsted-acid sites in 12-MR pockets as shown by infrared spectroscopy. The preferred temperature for delamination is 135 °C, based on increase in external surface area via N_2 physisorption, which is high enough to facilitate kinetics while being low enough to prevent significant formation of extra framework Al species as observed at higher treatment temperatures. A minor component of extra framework Al in the material delaminated at 135 °C was removed via a brief postsynthetic acid treatment. This dealumination led to stronger acid sites, when using infrared spectroscopic characterization of adsorbed pyridine and did not lead to amorphization as ascertained by PXRD, ^{29}Si NMR spectroscopy, and N_2 physisorption. A comparison of catalysis rates for the Friedel−Crafts acylation of 2-methox-ynaphthalene and acetic anhydride shows a 2.3-fold higher activity for this dealuminated and delaminated material, which is nearly equal to the observed increase in its external surface area, relative to the calcined 3D material ERB-1-C. Given the extraordinary simplicity and surfactant- and sonication-free nature of this mild delamination and B/Al exchange method, we expect it to find widespread utility for synthesis of delaminated zeolite catalysts for a variety of reactions.

ASSOCIATED CONTENT

Ⓢ Supporting Information

The whole-pattern profile-fitting of the PXRD patterns of ERB-1P, ERB-1C, and ERB-1-del-135; curvefitting of ^{29}Si MAS NMR spectra and calculation of the ratios of Q^3/Q^4 Si of ERB-1C, ERB-1-del-100, ERB-1-del-135, and ERB-1-del-175; TEM images characterizing ERB-1P; N_2 NLDFT differential pore volume plots over pore width distributions up to 1000 Å for ERB-1C and ERB-1-del-135; TGA data of ERB-1P and ERB-1-del-135. This material is available free of charge via the Internet at http://pubs.acs.org.

AUTHOR INFORMATION

Corresponding Authors
askatz@berkeley.edu
SIZO@chevron

Notes

The authors declare no competing financial interest.

REFERENCES

(1) Davis, M. E. *Chem.—Eur. J.* **1997**, *3*, 1745−1750.
(2) Jiang, J.; Yu, J.; Corma, A. *Angew. Chem., Int. Ed.* **2010**, *49*, 3120−3145.
(3) Corma, A.; Fornés, V.; Pergher, S. B.; Maesen, T. L. M.; Buglass, J. G. *Nature* **1998**, *396*, 353−356.
(4) Maheshwari, S.; Jordan, E.; Kumar, S.; Bates, F. S.; Penn, R. L.; Shantz, D. F.; Tsapatsis, M. *J. Am. Chem. Soc.* **2008**, *130*, 1507−1516.
(5) Ogino, I.; Nigra, M. M.; Hwang, S.-J.; Ha, J.-M.; Rea, T.; Zones, S. I.; Katz, A. *J. Am. Chem. Soc.* **2011**, *133*, 3288−3291.
(6) Eilertsen, E. A.; Ogino, I.; Hwang, S.-J.; Rea, T.; Yeh, S.; Zones, S. I.; Katz, A. *Chem. Mater.* **2011**, *23*, 5404−5408.
(7) Roth, W. J.; Čejka, J. *Catal. Sci. Technol.* **2011**, *1*, 43−53.
(8) Ogino, I.; Eilertsen, E. A.; Hwang, S.-J.; Rea, T.; Xie, D.; Ouyang, X.; Zones, S. I.; Katz, A. *Chem. Mater.* **2013**, *25*, 1502−1509.
(9) Choi, M.; Na, K.; Kim, J.; Sakamoto, Y.; Terasaki, O.; Ryoo, R. *Nature* **2009**, *461*, 246−249.
(10) Fan, W.; Snyder, M. A.; Kumar, S.; Lee, P.-S.; Yoo, W. C.; McCormick, A. V.; Penn, R. L.; Stein, A.; Tsapatsis, M. *Nat. Mater.* **2008**, *7*, 984−991.
(11) Na, K.; Jo, C.; Kim, J.; Cho, K.; Jung, J.; Seo, Y.; Messinger, R. J.; Chmelka, B. F.; Ryoo, R. *Science* **2011**, *333*, 328−332.
(12) Zhang, X.; Liu, D.; Xu, D.; Asahina, S.; Cychosz, K. A.; Agrawal, K. V.; Al Wahedi, Y.; Bhan, A.; Al Hashimi, S.; Terasaki, O.; Thommes, M.; Tsapatsis, M. *Science* **2012**, *336*, 1684−1687.
(13) Wang, L.; Wang, Y.; Liu, Y.; Chen, L.; Cheng, S.; Gao, G.; He, M.; Wu, P. *Microporous Mesoporous Mater.* **2008**, *113*, 435−444.
(14) Wang, Y.; Liu, Y.; Wang, L.; Wu, H.; Li, X.; He, M.; Wu, P. *J. Phys. Chem. C* **2009**, *113*, 18753−18760.
(15) Liu, G.; Jiang, J.-G.; Yang, B.; Fang, X.; Xu, H.; Peng, H.; Xu, L.; Liu, Y.; Wu, P. *Microporous Mesoporous Mater.* **2013**, *165*, 210−218.
(16) Roth, W. J.; Shvets, O. V.; Shamzhy, M.; Chlubná, P.; Kubu, M.; Nachtigall, P.; Čejka, J. *J. Am. Chem. Soc.* **2011**, *133*, 6130−6133.
(17) Verheyen, E.; Joos, L.; Van Havenbergh, K.; Breynaert, E.; Kasian, N.; Gobechiya, E.; Houthoofd, K.; Martineau, C.; Hinterstein, M.; Taulelle, F.; Van Speybroeck, V.; Waroquier, M.; Bals, S.; Van Tendeloo, G.; Kirschhock, C. E. A.; Martens, J. A. *Nat. Mater.* **2012**, *11*, 1059−1064.
(18) Chlubná, P.; Roth, W. J.; Greer, H. F.; Zhou, W.; Shvets, O.; Zukal, A.; Čejka, J.; Morris, R. E. *Chem. Mater.* **2013**, *25*, 542−547.
(19) Roth, W. J.; Nachtigall, P.; Morris, R. E.; Wheatley, P. S.; Seymour, V. R.; Ashbrook, S. E.; Chlubná, P.; Grajciar, L.; Položij, M.; Zukal, A.; Shvets, O.; Čejka, J. *Nat. Chem.* **2013**, *5*, 628−633.
(20) Millini, R.; Perego, G.; Bellussi, G. *Top. Catal.* **1999**, *9*, 13−34.
(21) Chen, C. Y.; Zones, S. I. In *Proceedings: 13th International Zeolite Conference*; Galarneau, A., Di Renzo, F., Fujula, F., Vedrine, J., Eds.; Elsevier: Amsterdam, 2001; p 26-O-05.
(22) Chen, C. Y.; Zones, S. I.; Hwang, S. J.; Bull, L. M. In *Proceedings: 14th International Zeolite Conference*; Van Steen, E., Claeys, M., Callanan, L. H., Eds.; Elsevier: Amsterdam, 2004; Vol. 154, pp 1547−1554.
(23) Chen, C. Y.; Zones, S. I. In *Proceedings: 13th International Zeolite Conference*; Galarneau, A., Di Renzo, F., Fujula, F., Vedrine, J., Eds.; Elsevier: Amsterdam, 2001, p 11-P-16.
(24) Liu, L.; Cheng, M.; Ma, D.; Hu, G.; Pan, X.; Bao, X. *Microporous Mesoporous Mater.* **2006**, *94*, 304−312.
(25) Dartt, C. B.; Davis, M. E. *Appl. Catal., A* **1996**, *143*, 53−73.

(26) Hamoudi, S.; Larachi, F.; Sayari, A. *Catal. Lett.* **2001**, *77*, 227−231.

(27) Wu, P.; Tatsumi, T. *Chem. Commun.* **2002**, 1026−1027.

(28) Deruiter, R.; Kentgens, A. P. M.; Grootendorst, J.; Jansen, J. C.; Van Bekkum, H. *Zeolites* **1993**, *13*, 128−138.

(29) Hwang, S. J.; Chen, C. Y.; Zones, S. I. *J. Phys. Chem. B* **2004**, *108*, 18535−18546.

(30) Gil, B.; Zones, S. I.; Hwang, S.-J.; Bejblová, M.; Čejka, J. *J. Phys. Chem. C* **2008**, *112*, 2997−3007.

(31) Millini, R.; Perego, G.; Parker, W. O.; Bellussi, G.; Carluccio, L. *Microporous Mater.* **1995**, *4*, 221−230.

(32) Zones, S. I.; Hwang, S.-J. *Microporous Mesoporous Mater.* **2011**, *146*, 48−56.

(33) Archer, R. H.; Zones, S. I.; Davis, M. E. *Microporous Mesoporous Mater.* **2010**, *130*, 255−265.

(34) Le Bail, A.; Duroy, H.; Fourquet, J. L. *Mater. Res. Bull.* **1988**, *23*, 447−452.

(35) Le Bail, A. *Powder Diffr.* **2005**, *20*, 316−326.

(36) Larson, A. C.; Von Dreele, R. B. *Los Alamos National Laboratory Report LAUR* **2000**, 86−748.

(37) Toby, B. H. *J. Appl. Crystallogr.* **2001**, *34*, 210−213.

(38) Thompson, P.; Cox, D. E.; Hastings, J. B. *J. Appl. Crystallogr.* **1987**, *20*, 79−83.

(39) Finger, L. W.; Cox, D. E.; Jephcoat, A. P. *J. Appl. Crystallogr.* **1994**, *27*, 892−900.

(40) Ravikovitch, P. I.; Haller, G. L.; Neimark, A. V. *Adv. Colloid Interface Sci.* **1998**, *76*, 203−226.

(41) Guisnet, M.; Ayrault, P.; Coutanceau, C.; Alvarez, M. F.; Datka, J. *J. Chem. Soc., Faraday Trans.* **1997**, *93*, 1661−1665.

(42) Roth, W. J.; Dorset, D. L. *Microporous Mesoporous Mater.* **2011**, *142*, 32−36.

(43) Lippmaa, E.; Maegi, M.; Samoson, A.; Engelhardt, G.; Grimmer, A. R. *J. Am. Chem. Soc.* **1980**, *102*, 4889−4893.

(44) Camblor, M. A.; Corell, C.; Corma, A.; Díaz-Cabañas, M. J.; Nicolopoulos, S.; González-Calbet, J. M.; Vallet-Regí, M. *Chem. Mater.* **1996**, *8*, 2415−2417.

(45) Camblor, M. A.; Corma, A.; Díaz-Cabañas, M. J.; Baerlocher, C. *J. Phys. Chem. B* **1998**, *102*, 44−51.

(46) Fild, C.; Shantz, D. F.; Lobo, R. F.; Koller, H. *Phys. Chem. Chem. Phys.* **2000**, *2*, 3091−3098.

(47) Tong, H. T. T.; Koller, H. *Microporous Mesoporous Mater.* **2012**, *148*, 80−87.

(48) Lawton, S. L.; Fung, A. S.; Kennedy, G. J.; Alemany, L. B.; Chang, C. D.; Hatzikos, G. H.; Lissy, D. N.; Rubin, M. K.; Timken, H. K. C.; Steuernagel, S.; Woessner, D. E. *J. Phys. Chem.* **1996**, *100*, 3788−3798.

(49) Kolodziejski, W.; Zicovichwilson, C.; Corma, A. *J. Phys. Chem.* **1995**, *99*, 7002−7008.

(50) Ma, D.; Deng, F.; Fu, R. Q.; Dan, X. W.; Bao, X. H. *J. Phys. Chem. B* **2001**, *105*, 1770−1779.

(51) Lakowicz, J. R.; Balter, A. *Biophys. Chem.* **1982**, *16*, 117−132.

(52) Corma, A.; Diaz, U.; Fornés, V.; Guil, J. M.; Martínez-Triguero, J.; Creyghton, E. J. *J. Catal.* **2000**, *191*, 218−224.

(53) Carr, R. T.; Neurock, M.; Iglesia, E. *J. Catal.* **2011**, *278*, 78−93.

(54) Corma, A.; Corell, C.; Pérez-Pariente, J. *Zeolites* **1995**, *15*, 2−8.

(55) Onida, B.; Borello, L.; Bonelli, B.; Geobaldo, F.; Garrone, E. *J. Catal.* **2003**, *214*, 191−199.

(56) Trombetta, M.; Armaroli, T.; Alejandre, A. G.; Solis, J. R.; Busca, G. *Appl. Catal., A* **2000**, *192*, 125−136.

(57) Corma, A.; Corell, C.; Fornés, V.; Kolodziejski, W.; Pérez-Pariente, J. *Zeolites* **1995**, *15*, 576−582.

(58) Loeffler, E.; Peuker, C.; Jerschkewitz, H. G. *Catal. Today* **1988**, *3*, 415−420.

(59) Ong, L. H.; Doemoek, M.; Olindo, R.; van Veen, A. C.; Lercher, J. A. *Microporous Mesoporous Mater.* **2012**, *164*, 9−20.

(60) Barzetti, T.; Selli, E.; Moscotti, D.; Forni, L. *J. Chem. Soc., Faraday Trans.* **1996**, *92*, 1401−1407.

(61) Jones, C. W.; Hwang, S. J.; Okubo, T.; Davis, M. E. *Chem. Mater.* **2001**, *13*, 1041−1050.

(62) Leonowicz, M. E.; Lawton, J. A.; Lawton, S. L.; Rubin, M. K. *Science* **1994**, *264*, 1910−1913.

(63) Chen, C. Y.; Xiao, S. Q.; Davis, M. E. *Microporous Mater.* **1995**, *4*, 1−20.

(64) Archer, R. H.; Carpenter, J. R.; Hwang, S.-J.; Burton, A. W.; Chen, C.-Y.; Zones, S. I.; Davis, M. E. *Chem. Mater.* **2010**, *22*, 2563−2572.

(65) Harrington, P. J.; Lodewijk, E. *Org. Process Res. Dev.* **1997**, *1*, 72−76.

(66) Sartori, G.; Maggi, R. *Chem. Rev.* **2006**, *106*, 1077−1104.

(67) Sartori, G.; Maggi, R. *Chem. Rev.* **2011**, *111*, PR181−PR214.

(68) Gunnewegh, E. A.; Gopie, S. S.; Van Bekkum, H. *J. Mol. Catal. A: Chem.* **1996**, *106*, 151−158.

(69) Harvey, G.; Mader, G. *Collect. Czech. Chem. Commun.* **1992**, *57*, 862−868.

(70) Heinichen, H. K.; Hölderich, W. F. *J. Catal.* **1999**, *185*, 408−414.

(71) Andy, P.; Garcia-Martinez, J.; Lee, G.; Gonzalez, H.; Jones, C. W.; Davis, M. E. *J. Catal.* **2000**, *192*, 215−223.

(72) Degnan, T. F., Jr.; Smith, C. M.; Venkat, C. R. *Appl. Catal., A* **2001**, *221*, 283−294.

(73) Degnan, T. F., Jr. *J. Catal.* **2003**, *216*, 32−46.

(74) Meric, P.; Finiels, A.; Moreau, P. *J. Mol. Catal. A: Chem.* **2002**, *189*, 251−262.

(75) Blumenfeld, A. L.; Coster, D.; Fripiat, J. J. *J. Phys. Chem.* **1995**, *99*, 15181−15191.